Growth structure and work function of bilayer graphene on Pd(111)

Y. Murata, S. Nie, A. Ebnonnasir, E. Starodub, B. B. Kappes, K. F. McCarty, C. V. Ciobanu, and S. Kodambaka

Growth Structure and Work Function of Bilayer Graphene on Pd(111)

Y. Murata[1], S. Nie[2], A. Ebnonnasir[3], E. Starodub[2], B. B. Kappes[3], K. F. McCarty[2], C. V. Ciobanu[3*], and S. Kodambaka[1*]

[1]*Department of Materials Science and Engineering, University of California Los Angeles, Los Angeles, CA 90095*
[2]*Sandia National Laboratories, Livermore, CA 94550*
[3]*Department of Mechanical Engineering and Materials Science Program, Colorado School of Mines, Golden, Colorado 80401*

Using *in situ* low-energy electron microscopy and density functional theory, we studied the growth structure and work function of bilayer graphene on Pd(111). Low-energy electron diffraction analysis established that the two graphene layers have multiple rotational orientations relative to each other and the substrate plane. We observed heterogeneous nucleation and simultaneous growth of multiple, faceted layers prior to the completion of second layer. We propose that the facetted shapes are due to the zigzag-terminated edges bounding graphene layers growing under the larger overlying layers. We also found that the work functions of bilayer graphene domains are higher than those of monolayer graphene, and depend sensitively on the orientations of both layers with respect to the substrate. Based on first-principles simulations, we attribute this behavior to oppositely oriented electrostatic dipoles at the graphene/Pd and graphene/graphene interfaces, whose strengths depend on the orientations of the two graphene layers.

PACS numbers:

I. INTRODUCTION

Few-layer graphene[1] is attractive for applications in optoelectronics as transparent conductors –where precise control over layer thickness is not necessary– owing to its low sheet resistance and high transparency,[2,3] and in field-effect transistors due to the opening of an electronic bandgap that, at least in bilayer graphene, can be tuned with an electric field.[4] Given that device characteristics depend on the work function of graphene and on how it varies at contacts,[5] it is of fundamental and practical importance to understand the nature of the contact (Ohmic or Schottky) at metal-graphene interfaces. In the case of monolayer graphene, recent studies indicate that the crystallographic orientation of graphene domains with respect to the metal can alter their electronic properties.[6–8] For few-layer graphene, the role of the specific metal surface and of the in-plane orientations of those layers on the electrical characteristics of the graphene is not well known. We choose Pd(111), one of the commonly used contact materials recently shown to exhibit low contact resistance,[5] as a model to investigate the influence of thickness and orientation on the work functions of graphene layers on metals.

Here, we present results of in situ low-energy electron microscopy (LEEM) and density functional theory (DFT) investigations of the growth structure and work function of bilayer graphene on Pd(111). Selected area low-energy electron diffraction (LEED) patterns indicate that Bernal stacking is typically not observed in the as-grown graphene layers. From the electron reflectivity data, we have extracted work functions of graphene domains as a function of the in-plane orientations of the top and bottom layers. For monolayer graphene, we have previously shown that the work functions can vary by up to 0.15 eV depending on the orientation of the domains with respect to the substrate.[7] Different registries between the graphene monolayer and the Pd(111) substrate lead to strong spatial variations of the charge transfer between the graphene and substrate. The resulting net surface dipole moment varies with the in-plane orientation of the monolayer. In case of bilayer graphene, we find that a smaller net electric dipole develops between the topmost graphene layer and the rest of the system (*i.e.*, the monolayer-covered substrate). The direction of this secondary dipole moment is opposite to that of the dipole developed at the Pd/graphene interface, and leads to an increase in the work function as compared to monolayer-covered Pd. Furthermore, the magnitude of the secondary dipole changes with the orientation of the second layer. This observation suggests that the first graphene layer does not fully passivate the substrate but allows charge transfer into the second layer, thus affecting the work function of the supported bilayer graphene.

II. EXPERIMENTAL METHODS AND RESULTS

A. Methods

All of our experiments are carried out using a carbon-saturated Pd(111) single crystal in an ultra-high vacuum (UHV, base pressure $< 1.0 \times 10^{-10}$ Torr) LEEM system.[9,10] Sample preparation and other experimental

---

details are presented in Ref. 7. Graphene layers of desired thickness are obtained by cooling from ~ 900 °C to lower temperatures, during which C segregates from the bulk to the surface.[11–13] For example, monolayer graphene is obtained when the sample is cooled from ~ 900 to ~ 790 °C at the rate of ~ 1 K/s. Upon completion of the first layer, further cooling to ~ 700 °C or lower yields multilayer graphene. Bright-field LEEM images are acquired as a function of time at the annealing temperature. The direct observation of graphene formation helps identify the layer thickness and is also useful in understanding the nucleation and growth kinetics. After the growth of a desired number of layers, the sample is quench-cooled to room temperature. LEEM images are then acquired as a function of electron energy E at 0.1 eV intervals between $E = -5$ and 30 eV and 0.01 eV intervals between $E = 0.0$ and 2.5 eV. From the LEEM image intensity I vs. E data, we determine the graphene layer thickness, the electron injection threshold energy ϕ, and the work function Φ.[14,15] Selected area LEED patterns[9] are used to identify the orientation θ of graphene layers with respect to the substrate. We define θ as the angle between Pd$[1\bar{1}0]$ and graphene$[11\bar{2}0]$ directions with the positive (negative) sign denoting in-plane, clockwise (counterclockwise) rotation. The measurement uncertainties in θ values are $\pm 1°$.
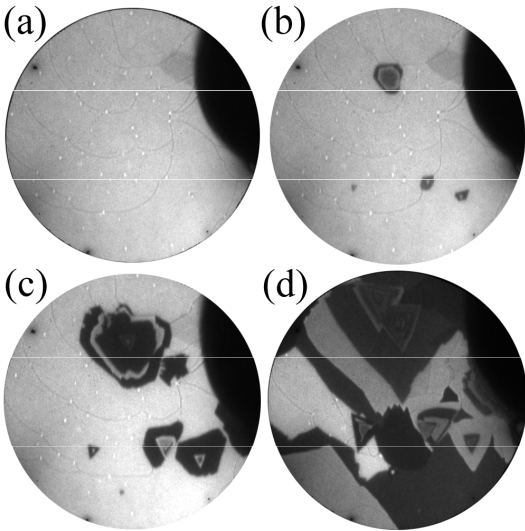
B. LEEM results

FIG. 1: Representative LEEM images of Pd(111) acquired after cooling from 790 °C to 660 °C during the growth of multilayer graphene at times $t =$ (a) 17 s, (b) 39 s, (c) 83 s, and (d) 205 s. ($t = 0$ corresponds to the time at which the sample temperature is 660 °C.) Field of view = 9.3 μm and electron energy $E = 4.3$ eV.

Figure 1 shows a series of bright-field LEEM images acquired from a Pd(111) sample during the growth of multilayer graphene at 660 °C. The sample is cooled from 790 °C when the surface was already covered with 1 ML graphene (Fig. 1a). The alternating brighter and darker grey features in Figs. 1b-d, as we show below, are multilayer stacks of graphene. (The black contrast region observed along the upper right corner of the LEEM images is due to a three-dimensional Pd mound on the surface.) We observe three interesting phenomena: (i) growth occurs at selected locations on the sample, suggestive of heterogeneous nucleation, presumably at surface defects; (ii) multiple layers nucleate and grow simultaneously, *i.e.*, third and higher layers appear before the completion of the second layer. In this measurement sequence, within 205 s of cooling to 660 °C, most of the nucleated sites are covered with ten or more layers of graphene at the nucleation sites (see Fig. 1d); and (iii) the multilayer domains are faceted with regular triangular and/or truncated hexagonal shapes, indicative of strong anisotropy in step energies.

We explain this observation as follows. Graphene's honeycomb lattice gives rise to two types of simple edge structures, armchair and zigzag. The angle between any two armchair or any two zigzag edges is 60° or 120°, and that between armchair and zigzag edges is 30° or 90°. Therefore, if the edges of the equilateral triangular and/or truncated hexagonal shapes are simple, they must all be either zigzag or armchair in structure. By comparing the directions of domain edges observed in the LEEM images with the LEED spot orientations, we determined that the domains are bounded by graphene sheets with zigzag edges. We suggest that asymmetries in the geometry of zigzag edges relative to an adjacent graphene layer may account for the anisotropic shapes of multilayer domains. The asymmetry is most easily illustrated for the case of two Bernal-stacked layers, as shown in Fig. 2. All of the armchair edges are equivalent. However, any two zigzag edges oriented at 120° to each other are not equivalent, analogous to the A- and B- type steps on (111)-oriented face-centered cubic crystals. As we describe in the next section, however, none of the observed graphene bilayer domains exhibit Bernal stacking (see Fig. 3). Yet, it is possible that the energies of both armchair and zigzag edges can vary with their orientation relative to the adjacent layer. This may explain the observation of multiple types of anisotropic shapes.

In the following sections, we report the thickness, crystallographic orientation, and work functions of the graphene layers. Fig. 3a is a representative LEEM image of multilayer graphene grown by cooling the sample from 900 °C to 709 °C and held for 1200 s. Fig. 3b is a typical plot of I vs. E data collected from the regions (color coded for clarity) highlighted in Fig. 3a. Note the oscillations in I at E values between ~ 1 and ~ 8 eV. These oscillations are a direct consequence of interference between electrons reflecting from the surface and those from interlayer and/or layer-substrate interfaces.[16] The
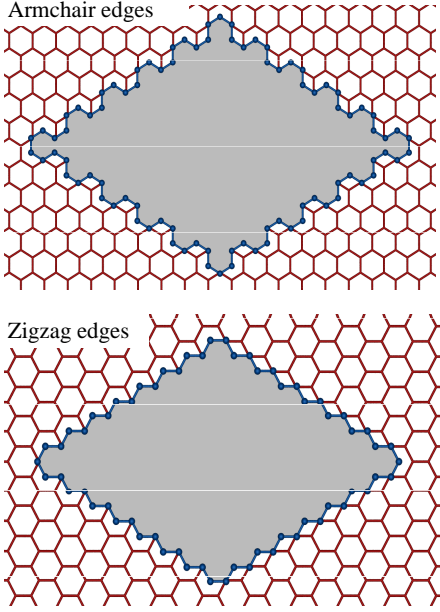
FIG. 2: Top-view schematic of Bernal-stacked bilayer graphene lattice. The top and bottom panels show the upper graphene domain bounded by armchair and zigzag edges, respectively. For clarity, the lower graphene layer is wider and shows the carbon network, while the upper layer shows only the edge atoms and their first neighbors.

FIG. 3: (a) Typical LEEM image of multilayer graphene on Pd(111). Field of view = 9.3 μm, E = 3.25 eV. (b) Image intensity I vs. E for multilayer graphene. (c-f) Selected area LEED patterns of 1, 2, 3, and 4 ML graphene-covered regions highlighted by blue, green, purple, and orange squares in (a), respectively. Red arrow in (c) indicates the Pd[$1\bar{1}0$]. The blue arrow indicates the graphene[$11\bar{2}0$] for the topmost-graphene sheet. The green and purple arrows indicate graphene[$11\bar{2}0$] for the buried graphene sheets that give the second strongest diffraction from 2 and 3 ML, respectively.

number of oscillations increases with increasing number of layers. For graphene on Pd(111), we find that n-layer graphene, irrespective of the interlayer stacking, exhibits (n-1) oscillations, $i.e.$, 1, 2, 3, and 4 ML show 0, 1, 2, and 3 oscillations, respectively (Fig. 3b). This result is similar to the I vs. E data for multilayer graphene on SiC(0001) after accounting for the so-called "buffer" layer.[16,17]

C. LEED results

Next, we have determined the crystallographic orientations of the individual graphene layers using selected area LEED in combination with I vs. E data. Figs. 3c-f are representative LEED patterns acquired from the regions, highlighted in Fig. 3a, of 1, 2, 3, and 4 ML graphene analyzed above. We first identify the diffraction spots corresponding to Pd(111). Of all the LEED patterns in Figs. 3c-f, only Fig. 3c shows six-fold symmetric spots corresponding to the Pd(111)-1 × 1 lattice. The other set of spots in Fig. 3c are due to the monolayer graphene-1×1 lattice, which is rotated with respect to the substrate by $\theta = -14°$. This data serves as the reference for the identification of LEED spots corresponding to 2, 3, and 4 ML graphene in Figs. 3d-f. Since the LEED spot intensity decreases with increasing distance into the surface, we can determine the position of the graphene layer with respect to the surface.
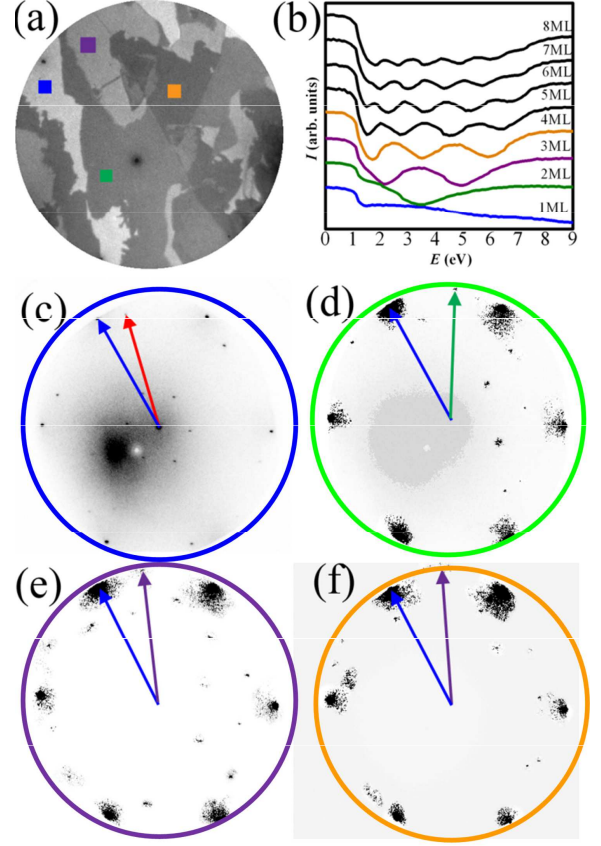
For example, in Fig. 3d, we observe two sets of six-fold symmetric spots due to bilayer graphene, with the stronger and weaker intensity spots oriented along $\theta = -14°$ and $\theta = +14°$, respectively. That is, the top graphene layer is oriented along $\theta_1 = -14°$ while the layer closer to the substrate is along $\theta_2 = +14°$. The LEED patterns from 3 and 4 ML graphene, in Figs. 3e and 3f, respectively also show two sets of six-fold symmetric spots with the strongest spots along $\theta = -14°$ and the weaker spots along $\theta = +8.9°$. We identify $\theta = -14°$ as the topmost layer, in both Figs. 3e and 3f. However, we could not determine which of the underlying graphene layers gives rise to the $\theta = +8.9°$ spots. In all of the LEED patterns, we find that one of the layers in multilayer graphene is oriented at the same angle ($\theta = -14°$ in the example of Fig. 3) as in the 1 ML graphene that
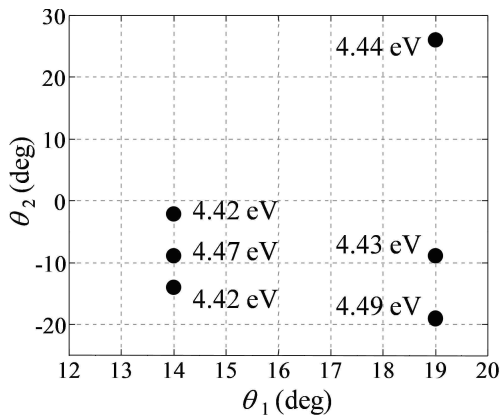
FIG. 4: Experimental work function values for bilayer graphene on Pd(111) for different orientations θ_1 and θ_2 of the two graphene layers.

surrounds the multilayer stack. This observation suggests that orientation of the top layer graphene is unaffected during the growth of subsequent layers, consistent with the expected growth of multiple layers below the layer that grows first.[18] From LEED patterns acquired from over 10 different regions of the sample, we identified at least 12 different in-plane orientations in bilayer graphene. In all cases the two layers are not rotationally aligned, as required for Bernal stacking, similar to previous reports.[7] Based upon our data, we suggest that Bernal stacking will be rare in graphene layers grown on Pd(111).

D. Work function of graphene bilayers on Pd

We now focus on the relationship between work function Φ and orientation of bilayer graphene. Following the procedure outlined in Ref. 7, we first measure the electron injection threshold energy ϕ, at which the image intensity I drops to 90% of the intensity value at $E = 0$ eV. Then, $\Phi = \Phi_{fil} + \phi$, where Φ_{fil} is the work function of the electron gun filament. From the I vs. E data obtained from clean Pd(111) along with known values of Φ for Pd ($5.3-5.6$ eV),[7] we estimate Φ_{fil} to be between 3.1 and 3.4 eV. Given the large uncertainties in the knowledge of Φ_{fil} (up to 0.3 eV), we do not emphasize determining absolute values of Φ. However, ϕ values are precise to within 0.02 eV and, therefore, can be used to compare how Φ changes with orientation and layer thickness. Recently, we reported that Φ of monolayer graphene on Pd(111) varies with in-plane rotation due to spatial variations in charge transfer at graphene - Pd interface.[7] Using the same approach and assuming that $\Phi_{fil} = 3.4$ eV, we have determined Phi for bilayer graphene domains as a function of θ_1 and θ_2.

Fig. 4 shows the work function values Φ for bilayer graphene plotted at different values of θ_1 and θ_2. For all domain orientations, the work function of bilayer graphene is higher than that for monolayer graphene. Our results for Φ of graphene bilayers on Pd(111) are similar to recent reports on epitaxial graphene grown on SiC (where the Φ of bilayer graphene is also higher than that of a monolayer),[19] but opposite to those for free-standing graphene transferred onto SiO_2,[20] where Φ is found to decrease with increasing layer thickness. We note, however, that the effect of domain orientation on the Φ values of bilayer graphene on Pd(111) is smaller (up to 0.07 eV) compared to that observed (up to 0.15 eV) in Φ for monolayer graphene domains (see Fig. 4). In order to confirm these results, we determined Φ values using a different procedure,[14,15] and obtained consistent results. An important factor that affects the work function of bilayer graphene is the in-plane orientation of the two layers, which we next discuss from the perspective of electronic structure calculations.

III. DFT RESULTS AND DISCUSSION

In order to gain insights into how the second graphene layer and the orientation of both layers affect the work function, we have performed DFT calculations on systems with one and two graphene layers placed on one side of a Pd(111) substrate. We have used the Siesta code[21] with double-zeta (DZ) basis set within the local density approximation (LDA) with the Ceperley-Alder exchange-correlation functional. A uniform grid in real space with a mesh cutoff of 150 Ry was used. The Brillouin zone has been sampled only at the Γ point since the unit cells were large, with periodicity vectors of 19.72Å. The residual forces on any atom are smaller than 0.04 eV/Å at the end of structural relaxations, and the total energy has been converged to within 10^{-5} eV for all electronic property calculations. We have used 8×8 surface supercells for the construction of 19.9° and 30°-rotated graphene domains (126 C atoms and 128 C atoms, respectively), and 46 Pd atoms per layer with four Pd layers in the substrate. For the 30° orientation, we have adopted the epitaxial structure proposed by Giovanetti et al.[22] The choice of the two particular orientations, 19.9° and 30°, is determined both by the necessity to keep the computations tractable and by the fact that these two orientations can be placed simultaneously on the Pd(111) substrate with virtually no strain in either of them. Thus, any computed variations in Φ are due only to their orientations and/or stacking order, but not to the (insignificant) strain in the graphene layers.

For monolayer graphene, we compute the charge transfer and the associated dipole moment in a manner similar to previous reports,[23] but strictly adopt the standard direction convention for electrostatic dipole (i.e., dipole vector pointing from the negative charge to the positive charge). For single- and bi-layer graphene, the planar averaged electron density transferred with respect to all the individual components (substrate, first layer, and second

TABLE I: Work function results from DFT calculations for single- and bi-layer graphene, along with the net dipole P_a and the secondary dipole P_b defined in text. The work function of pure Pd substrate is also given as a reference. The electronic transfer to the graphene layer(s) is given in the last column, where 1st layer denotes the one closest to the Pd substrate.

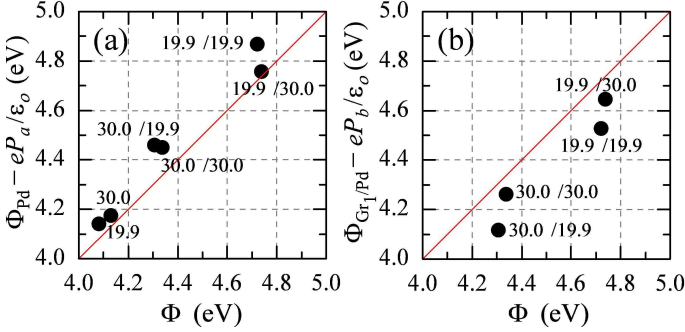| System	Work Function (eV)	Net dipole P_a (D/Å^2)	Secondary dipole, P_b (D/Å^2)	Electrons transferred (e/Å^2) 1st layer [2nd layer]
Pd	5.165	—	—	—
30.0°/Pd	4.131	+0.027	—	-0.0027
19.9°/Pd	4.082	+0.027	—	-0.0023
30.0°/19.9°/Pd	4.307	+0.019	-0.001	-0.0029 [+0.0003]
19.9°/30.0°/Pd	4.738	+0.011	-0.014	-0.0056 [+0.0027]
30.0°/30.0°/Pd	4.337	+0.019	-0.003	-0.0041 [+0.0009]
19.9°/19.9°/Pd	4.723	+0.008	-0.012	-0.0048 [+0.0023]

FIG. 5: Work function values from dipole moment calculations, $\Phi_{ref} - eP/\epsilon_0$, vs. values determined directly from DFT calculations, Φ. (a) Bare Pd surface is taken as the reference for single- and bi-layer epitaxial systems. (b) Pd substrate covered with monolayer graphene is used as reference for the bi-layer calculations.

layer –when present), is defined by

$$\Delta\rho_a(z) = \rho_{Gr_2/Gr_1/Pd}(z) - \rho_{Pd}(z) - \rho_{Gr_1}(z) - \rho_{Gr_2}(z). \quad (1)$$

This electron transfer creates a net dipole moment when integrated from the middle of the substrate to the middle of the vacuum in the supercell, $P_a = \int z\Delta\rho_a(z)\mathrm{d}z$, dipole which should be responsible for the change in Φ with respect to the bare Pd surface

$$\Phi_{Gr_2/Gr_1/Pd} = \Phi_{Pd} - eP_a/\epsilon_0. \quad (2)$$

Indeed, computing the work function directly from the electrostatic potential output of the DFT simulation ($= \Phi_{vacuum} - E_{Fermi}$) and from the dipole moment P_a [via Eq. (2)] shows that the electrostatic dipole largely accounts for the work function of single- and bi-layer graphene on Pd (Fig. 5a). For both single- and bi-layer graphene, the values of the dipole moment P_a are positive (*i.e.*, pointing away from the substrate, see Table 1) and of same order of magnitude as that reported for other graphene-metal systems.[23]

To account specifically for the influence of the second graphene layer on Φ, we resort to another way of computing the dipole moment, one in which the reference consists of the topmost (second) graphene layer and the palladium substrate covered with monolayer graphene,

$$\Delta\rho_b(z) = \rho_{Gr_2/Gr_1/Pd}(z) - \rho_{Gr_1/Pd}(z) - \rho_{Gr_2}(z). \quad (3)$$

The charge transfer $\Delta\rho_b(z)$ and the dipole moment $P_b = \int z\Delta\rho_b(z)\mathrm{d}z$ developed with respect to the new reference are, therefore, much smaller when compared to the transfer to the first layer, as shown in Fig. 6 and listed in Table 1. Although smaller, the secondary dipole moment P_b does account for the work function changes between the single- and bi- layer graphene on Pd,

$$\Phi_{Gr_2/Gr_1/Pd} = \Phi_{Gr_1/Pd} - eP_b/\epsilon_0, \quad (4)$$

as seen in Fig. 4b. The secondary dipole moment P_b (Table 1) is always negative (*i.e.*, it points into the substrate), which explains our observation that the work functions of bilayer systems are greater than those of monolayer systems. We note that although the variations in experimentally measured values are in qualitative agreement with the DFT variations, they are smaller than those obtained using DFT. Possible reasons for the smaller variations in experimental values are (a) different orientations used in calculations compared to experiments (our initial attempts to use the experimental orientations in DFT simulations resulted in supercells that were either too large or too strained), and (b) the presence of elastic strain, carbon adatoms at the graphene-Pd interface, or other impurities in graphene layers.

Finally, we have also estimated the electron transfer to each graphene layer by integrating the density using as integration limits the midpoints between atomic layers. For computing the electron transfer to the second graphene layer (topmost), we integrated from the midpoint between the first and second graphene layers to the middle of the vacuum. The results, listed in the last column of Table 1, show that the first graphene layer is *p*-doped (loss of electrons), while the second layer is
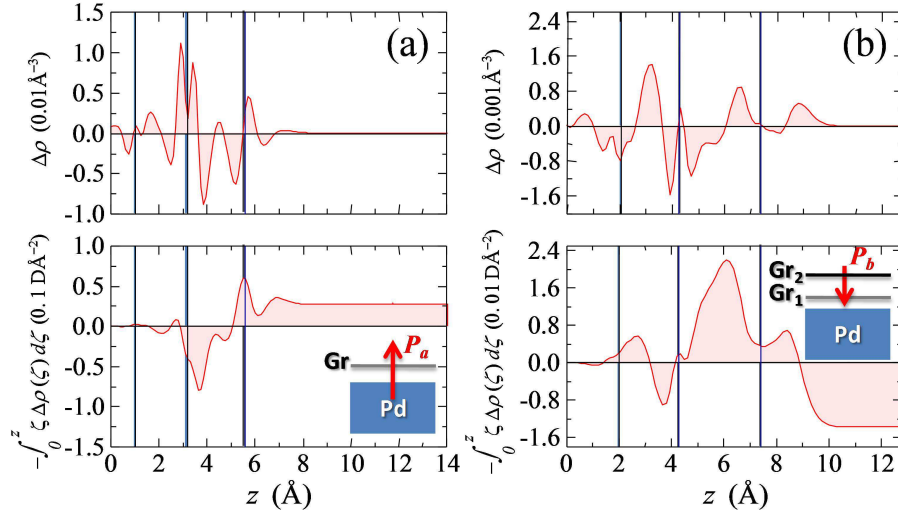
FIG. 6: Plane-averaged electron density transferred (number of electrons per unit volume) and surface dipole densities for (a) $30.0°$/Pd and (b) $19.9°$/$30.0°$/Pd. The vertical gray (blue) lines indicate the locations of the graphene (substrate) layers. The origin of the z coordinate is taken in the middle of the corresponding reference substrates, $i.e.$, (a) the midpoint of the bare Pd slab, and (b) the midpoint of the segment between inner (first) graphene layer and bare Pd layer on the opposite side of the slab. The arrows in the insets show schematically (a) the surface dipole along the surface normal for monolayer graphene, and (b) the secondary dipole pointing opposite to the surface normal.

n-doped. As seen in Table 1, the magnitude of the electron transfer to the second layer is relatively small and can be attributed to charge screening by the first layer.[24] The signs of the estimated electronic transfer to each graphene layer are certainly consistent with directions of the calculated dipoles P_a and P_b, $i.e.$, a loss of electrons on the first graphene layer leads to a dipole P_a parallel to the surface normal, while a gain of electrons on the second graphene layers leads to a secondary dipole P_b antiparallel to the surface normal.

IV. CONCLUSIONS

In conclusion, we used in $situ$ LEEM and DFT to investigate the growth structure and work function of multilayer graphene on Pd(111). None of the bilayer domains we examined had the rotational alignment required for Bernal stacking. Instead, there are multiple orientations of the layers relative to the substrate and each other. The orientation-dependent variations in work functions of bilayer graphene are relatively smaller than those observed in monolayer graphene. We explain these results using DFT calculations, which reveal that the charge transfer from Pd depends sensitively on the orientations of both graphene layers. Our results indicate that one cannot infer how multilayers of graphene interact with a metal substrate (for example, in a contact) by examining only the first layer. Therefore, for the fabrication of graphene-based transistors and/or transparent conductors, knowledge of the graphene layer stacking and its influence on the device characteristics is desirable.

[1] A. K. Geim and K. S. Novoselov, Nature Materials 6, 183 (2007).

[2] K. S. Kim, Y. Zhao, H. Jang, S. Y. Lee, J. M. Kim, J. H. Ahn, P. Kim, J. Y. Choi and B. H. Hong, Nature 457, 706 (2009).

[3] S. Bae, H. Kim, Y. Lee, X. F. Xu, J. S. Park, Y. Zheng, J. Balakrishnan, T. Lei, H. R. Kim, Y. I. Song, Y. J. Kim, K. S. Kim, B. Ozyilmaz, J. H. Ahn, B. H. Hong and S. Iijima, Nature Nanotechnology 5, 574 (2010).

[4] Y. B. Zhang, T. T. Tang, C. Girit, Z. Hao, M. C. Martin, A. Zettl, M. F. Crommie, Y. R. Shen and F. Wang, Nature 459, 820 (2009).

[5] F. N. Xia, V. Perebeinos, Y. M. Lin, Y. Q. Wu and P. Avouris, Nature Nanotechnology 6, 179 (2011).

[6] S. Y. Kwon, C. V. Ciobanu, V. Petrova, V. B. Shenoy, J. Bareno, V. Gambin, I. Petrov and S. Kodambaka, Nano Letters 9, 3985 (2009).

[7] Y. Murata, E. Starodub, B. B. Kappes, C. V. Ciobanu, N. C. Bartelt, K. F. McCarty and S. Kodambaka, Applied Physics Letters 97, 143114 (2010).

[8] Y. Murata, V. Petrova, B.B. Kappes, A. Ebnonnasir, I. Petrov, Y.-H. Xie, C.V. Ciobanu, and S. Kodambaka, ACS Nano 4, 6509 (2010)

[9] E. Loginova, N. C. Bartelt, P. J. Feibelman and K. F. McCarty, New Journal of Physics 11, 063046 (2009).

[10] K. F. McCarty, Surface Science 474, L165 (2001).

[11] C. Oshima and A. Nagashima, Journal of Physics-Condensed Matter 9, 1 (1997), and references therein.

[12] J. C. Hamilton and J. M. Blakely, Surface Science 91, 199 (1980).

[13] K. F. McCarty, P. J. Feibelman, E. Loginova and N. C. Bartelt, Carbon 47, 1806 (2009).

[14] M. Babout, M. Guivarch, R. Pantel, M. Bujor and C. Guittard, Journal of Physics D-Applied Physics 13, 1161 (1980).

[15] M. Babout, J. C. Lebosse, J. Lopez, R. Gauthier and C. Guittard, Journal of Physics D-Applied Physics 10, 2331 (1977).

[16] H. Hibino, H. Kageshima, F. Maeda, M. Nagase, Y. Kobayashi and H. Yamaguchi, Physical Review B 77, 075413 (2008).

[17] T. Ohta, F. El Gabaly, A. Bostwick, J. L. McChesney, K. V. Emtsev, A. K. Schmid, T. Seyller, K. Horn and E. Rotenberg, New Journal of Physics 10, 023034 (2008).

[18] S. Nie, A. L. Walter, N. C. Bartelt, E. Starodub, A. Bostwick, E. Rotenberg and K. F. McCarty, ACS Nano 5, 2298 (2011).

[19] T. Filleter, K. V. Emtsev, T. Seyller and R. Bennewitz, Applied Physics Letters 93, 133117 (2008).

[20] N. J. Lee, J. W. Yoo, Y. J. Choi, C. J. Kang, D. Y. Jeon, D. C. Kim, S. Seo and H. J. Chung, Applied Physics Letters 95, 222107 (2009).

[21] J. M. Soler, E. Artacho, J. D. Gale, A. Garcia, J. Junquera, P. Ordejon and D. Sanchez-Portal, Journal of Physics-Condensed Matter 14, 2745 (2002).

[22] G. Giovannetti, P. A. Khomyakov, G. Brocks, V. M. Karpan, J. van den Brink and P. J. Kelly, Physical Review Letters 101, 026803 (2008).

[23] B. Wang, S. Günther, J. Wintterlin and M. L. Bocquet, New Journal of Physics 12, 043041 (2010).

[24] D. Sun, C. Divin, C. Berger, W. A. de Heer, P. N. First and T. B. Norris, Physical Review Letters 104, 136802 (2010).